OPEN ACCESS

University of BRISTOL

Peer reviewed version

Link to published version (if available):
10.1364/OME.5.002174

Link to publication record in Explore Bristol Research
PDF-document

University of Bristol - Explore Bristol Research
General rights

Magnetically tunable non-reciprocal plasmons resonator based on graphene-coated nanowire

Bofeng Zhu,[1,2,3] Guobin Ren,[1,2,*] Martin J. Cryan,[3] Yixiao Gao,[1,2] Yang Yang,[4] Beilei Wu,[1,2] Yudong Lian,[1,2] and Shuisheng Jian[1,2]

[1]*Key Lab of All Optical Network & Advanced Telecommunication Network of EMC, Beijing Jiaotong University, Beijing 100044, China*
[2]*Institute of Lightwave Technology, Beijing Jiaotong University, Beijing 100044, China*
[3]*Department of Electrical and Electronic Engineering, University of Bristol, Bristol, UK*
[4]*Department of Physics, College of Science, Tianjin University of Technology, Tianjin 300191, China*
*gbren@bjtu.edu.cn.

Abstract: In this paper we propose a magnetically tunable plasmons resonator based on a graphene-coated nanowire. Due to the magneto-optical effect under an external magnetic field, the circumferential propagation of graphene plasmons on a magneto-optical nanowire becomes non-reciprocal with the modal indices depend on plasmons traveling directions (clockwise or anti-clockwise). When coupled with a graphene sheet waveguide, the two components form a graphene plasmons filter for which the shift direction of transmittance spectrum is determined by the direction of input plasmons. The resonant wavelengths of resonator are obtained through resonant cavity theory and verified by numerical solutions. Furthermore, the non-reciprocal transmittance enables such structures to achieve the function of a plasmons isolator where the isolation could be tuned by the amplitude of an external magnetic field and the enabled plasmons propagation direction could be switched by reversing the direction of external magnetic field. Under proper structural parameters and magnetic field, an isolation ratio over 25 dB is obtained. The proposed magnetically tunable plasmons resonator may provide new inspiration to graphene plasmonics devices.

References and links

1. K. S. Novoselov, A. K. Geim, S. V. Morozov, D. Jiang, M. I. Katsnelson, I. V. Grigorieva, S. V. Dubonos, and A. A. Firsov, "Two-dimensional gas of massless Dirac fermions in graphene," Nature **438**, 197-200 (2005).
2. A. N. Grigorenko, M. Polini, and K. S. Novoselov, "Graphene plasmonics," Nature Photonics **6**, 749-758 (2012).
3. W. B. Lu, W. Zhu, H. J. Xu, Z. H. Ni, Z. G. Dong, and T. J. Cui, "Flexible transformation plasmonics using graphene," Optics express **21**, 10475-10482 (2013).
4. Z. Fei, A. S. Rodin, G. O. Andreev, W. Bao, A. S. McLeod, M. Wagner, L. M. Zhang, Z. Zhao, M. Thiemens, G. Dominguez, M. M. Fogler, A. H. Castro Neto, C. N. Lau, F. Keilmann, and D. N. Basov, "Gate-tuning of graphene plasmons revealed by infrared nano-imaging," Nature **487**, 82-85 (2012).
5. D. Rafizadeh, J. P. Zhang, R. C. Tiberio, and S. T. Ho, "Propagation loss measurements in semiconductor microcavity ring and disk resonators," J Lightwave Technol **16**, 1308-1314 (1998).
6. A. Delage, D.-X. Xu, R. W. McKinnon, E. Post, P. Waldron, J. Lapointe, C. Storey, A. Densmore, S. Janz, B. Lamontagne, P. Cheben, and J. H. Schmid, "Wavelength-Dependent Model of a Ring Resonator Sensor Excited by a Directional Coupler," J Lightwave Technol **27**, 1172-1180 (2009).
7. T. B. Wang, X. W. Wen, C. P. Yin, and H. Z. Wang, "The transmission characteristics of surface plasmon polaritons in ring resonator," Optics express **17**, 24096-24101 (2009).
8. B. Maune, R. Lawson, C. Gunn, A. Scherer, and L. Dalton, "Electrically tunable ring resonators incorporating nematic liquid crystals as cladding layers," Applied Physics Letters **83**, 4689 (2003).
9. K. A. Boulais, D. W. Rule, S. Simmons, F. Santiago, V. Gehman, K. Long, and A. Rayms-Keller, "Tunable split-ring resonator for metamaterials using photocapacitance of semi-insulating GaAs," Applied Physics Letters **93**, 043518 (2008).

10. P. Heimala, P. Katila, J. Aarnio, and A. Heinamaki, "Thermally tunable integrated optical ring resonator with poly-Si thermistor," J Lightwave Technol **14**, 2260-2267 (1996).
11. Y. Gao, G. Ren, B. Zhu, H. Liu, Y. Lian, and S. Jian, "Analytical model for plasmon modes in graphene-coated nanowire," Optics express **22**, 24322-24331 (2014).
12. Y. Gao, G. Ren, B. Zhu, J. Wang, and S. Jian, "Single-mode graphene-coated nanowire plasmonic waveguide," Optics letters **39**, 5909-5912 (2014).
13. B. Zhu, G. Ren, Y. Gao, Y. Yang, B. Wu, Y. Lian, and S. Jian, "Nanofocusing in the graphene-coated tapered nanowire infrared probe," Journal of the Optical Society of America B **32**, 955 (2015).
14. F. Liu, C. Qian, and Y. D. Chong, "Directional excitation of graphene surface plasmons," Optics express **23**, 2383-2391 (2015).
15. W. Li, B. Chen, C. Meng, W. Fang, Y. Xiao, X. Li, Z. Hu, Y. Xu, L. Tong, H. Wang, W. Liu, J. Bao, and Y. R. Shen, "Ultrafast all-optical graphene modulator," Nano letters **14**, 955-959 (2014).
16. Y. Wu, B. Yao, A. Zhang, Y. J. Rao, Z. Wang, Y. Cheng, Y. Gong, W. Zhang, Y. Chen, and K. Chiang, "Graphene-coated microfiber Bragg grating for high sensitivity gas sensing," Optics letters **39**, 1235-1237 (2014).
17. H. Xiaoying, Z. Xiangchao, Z. Hao, and X. Min, "Graphene Covered on Microfiber Exhibiting Polarization and Polarization-dependent Saturable Absorption," IEEE Journal of Selected Topics in Quantum Electronics **20**, 4500107-4500107 (2014).
18. X. He, Z.-b. Liu, D. N. Wang, M. Yang, T. Y. Hu, and J.-G. Tian, "Saturable Absorber Based on Graphene-Covered-Microfiber," IEEE Photonics Technology Letters **25**, 1392-1394 (2013).
19. L. A. Falkovsky, "Optical properties of graphene and IV–VI semiconductors," Physics-Uspekhi **51**, 887-897 (2008).
20. W. Gao, J. Shu, C. Qiu, and Q. Xu, "Excitation of plasmonic waves in graphene by guided-mode resonances," ACS nano **6**, 7806-7813 (2012).
21. K. S. Novoselov, A. K. Geim, S. V. Morozov, D. Jiang, Y. Zhang, S. V. Dubonos, I. V. Grigorieva, and A. A. Firsov, "Electric field effect in atomically thin carbon films," Science **306**, 666-669 (2004).
22. M. Jablan, H. Buljan, and M. Soljacic, "Plasmonics in graphene at infrared frequencies," Physical Review B **80**, 7 (2009).
23. J. Tao, X. Yu, B. Hu, A. Dubrovkin, and Q. J. Wang, "Graphene-based tunable plasmonic Bragg reflector with a broad bandwidth," Optics letters **39**, 271-274 (2014).
24. B. Biel, F. Triozon, X. Blase, and S. Roche, "Chemically induced mobility gaps in graphene nanoribbons: a route for upscaling device performances," Nano letters **9**, 2725-2729 (2009).
25. V. Zayets, H. Saito, K. Ando, and S. Yuasa, "Optical Isolator Utilizing Surface Plasmons," Materials **5**, 857-871 (2012).
26. J. Brion, R. Wallis, A. Hartstein, and E. Burstein, "Theory of Surface Magnetoplasmons in Semiconductors," Physical Review Letters **28**, 1455-1458 (1972).
27. X. Miao, B. Passmore, A. Gin, W. Langston, S. Vangala, W. Goodhue, E. Shaner, and I. Brener, "Doping tunable resonance: Toward electrically tunable mid-infrared metamaterials," Applied Physics Letters **96**, 101111 (2010).
28. S. D. Parker, R. L. Williams, R. Droopad, R. A. Stradling, K. W. J. Barnham, S. N. Holmes, J. Laverty, C. C. Phillips, E. Skuras, R. Thomas, X. Zhang, A. Staton-Bevan, and D. W. Pashley, "Observation and control of the amphoteric behaviour of Si-doped InSb grown on GaAs by MBE," Semiconductor Science and Technology **4**, 663-676 (1989).
29. R. A. Stradling and R. A. Wood, "The temperature dependence of the band-edge effective masses of InSb, InAs and GaAs as deduced from magnetophonon magnetoresistance measurements," Journal of Physics C: Solid State Physics **3**, L94-L99 (1970).
30. I. Crassee, M. Orlita, M. Potemski, A. L. Walter, M. Ostler, T. Seyller, I. Gaponenko, J. Chen, and A. B. Kuzmenko, "Intrinsic terahertz plasmons and magnetoplasmons in large scale monolayer graphene," Nano letters **12**, 2470-2474 (2012).
31. C. M. Jaworski, R. C. Myers, E. Johnston-Halperin, and J. P. Heremans, "Giant spin Seebeck effect in a non-magnetic material," Nature **487**, 210-213 (2012).
32. L. P. Rokhinson, X. Liu, and J. K. Furdyna, "The fractional a.c. Josephson effect in a semiconductor–superconductor nanowire as a signature of Majorana particles," Nat Phys **8**, 795-799 (2012).
33. N. A. Pike and D. Stroud, "Model for the spin-dependent Seebeck coefficient of InSb in a magnetic field," Physical Review B **90**(2014).
34. D. L. Sounas, H. S. Skulason, H. V. Nguyen, A. Guermoune, M. Siaj, T. Szkopek, and C. Caloz, "Faraday rotation in magnetically biased graphene at microwave frequencies," Applied Physics Letters **102**, 191901 (2013).
35. M. Tamagnone, A. Fallahi, J. R. Mosig, and J. Perruisseau-Carrier, "Fundamental limits and near-optimal design of graphene modulators and non-reciprocal devices," Nature Photonics **8**, 556-563 (2014).
36. D. L. Sounas and C. Caloz, "Graphene-based non-reciprocal spatial isolator," 1597-1600 (2011).

1.   Introduction

Graphene is a semiconductor with a two-dimensional form of carbon atoms arranged in the honeycomb lattice [1]. Increasing attention has been paid to graphene due to its unique

mechanical, electric, magnetic properties, extremely high quantum efficiency for light-matter interactions and its ability to support graphene plasmons (GPs) with unusual properties [2]. For instance, the GPs supported on rigid curved graphene waveguides have shown much stronger confinement and smaller radiation loss than counterpart on noble metals [3]. On the other hand, graphene also presents strong tunability via electrical biasing [4], which leads to various tunable graphene-based devices. Ring resonators have been extensively studied and shown to possess distinct functionalities in integrated optics on a variety of platforms, such as semiconductors [5], high index contrast dielectric waveguide [6] and metal-insulator-metal (MIM) waveguides [7]. Recently, various tunable resonators have been proposed and demonstrated to achieve tunable resonances using nematic liquid crystals [8], the photo-capacitance of semi-insulating GaAs [9] or the thermo-optical effect [10].

Previously, a graphene-coated nanowire (GNW) waveguide structure has been proposed [11] and the longitudinal propagation of plasmons on a GNW waveguide has been clarified [12, 13]. Nevertheless, the circumferential propagation of GPs on a GNW has not been addressed yet, especially when the GNW is coupled with a graphene sheet waveguide. Meanwhile, although graphene itself has shown potentials of tunability, it is challenging to implement electrical bias on a GNW resonator to dynamically control its functionalities due to its geometric features. Therefore an alternative path is in demand to achieve tunable GNW resonators and other plasmons devices based on such structures. Significantly, in a recent study on directional excitation of GPs on magneto-optical substrates [14], the GPs dispersion relations possess non-reciprocal properties and can be tuned by an external magnetic field. Therefore, by combining with the magneto-optical effect, a new possibility can be expected to dynamically control the functionalities of devices based on the GNW structure.

In this paper we propose a magnetically tunable non-reciprocal plasmons resonator based on a graphene-coated InSb nanowire. In Sec. II we give justifications for the modelling parameters of plasmons filter based on a GNW being coupled to a graphene sheet waveguide. The modal indices of GPs along two opposite circumferential directions on GNW are presented. Then in Sec. III we illustrate the transmittance spectrum of the filter for opposite plasmons input directions and give justifications upon the device performances. The resonant cavity theory is adopted to describe resonant wavelengths, which are verified by numerical simulations. In Sec. IV, we propose that the non-reciprocal plasmons filter can be also regarded as a plasmons isolator, the isolation ratio with respect to the incident wavelength, external magnetic field, ring radius and chemical potential are investigated. Finally we draw conclusions.

2. The plasmons resonator based on graphene-coated InSb nanowire

Recently, it has been experimentally demonstrated that a graphene flake can be transferred onto a microfiber using adhesive tape and methyl isobutyl ketone [15]. Meanwhile, it has been shown that the graphene layer can be tightly coated onto a nanowire due to van der Waals forces [16-18]. Sketched in Fig. 1 are the schematics of the plasmons resonators composed of one graphene-coated doped InSb nanowire and one graphene sheet waveguide. Both two components are embedded in the dielectric medium with permittivity ε_1=3. The environment temperature is T=300 K with external magnetic field B along the z^+ direction. Either of the two ports could be the input port for graphene plasmons [shown in Figs. 1(a) and 1(b) respectively].
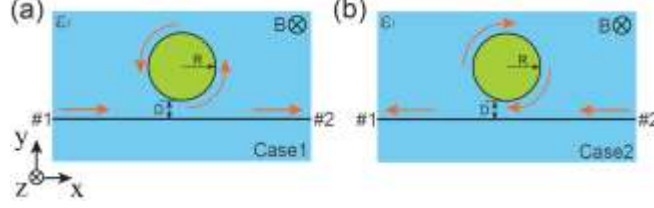
Fig. 1. Schematic of the proposed structure on plane *xy* with plasmons input from Port #1 along *x*[+] direction (a) and Port #2 along *x*[-] direction (b). The plasmons traveling directions on GNW structure are shown via orange arrows, *i.e.* anti-clockwise in (a) and clockwise in (b). The green region is the InSb nanowire and an external magnetic field *B* is parallel to *z* axis.

Through our discussion, the interspace between nanowire and waveguide is fixed at *D*=30 nm. The nanowire radius is *R*=100 nm and the length of graphene waveguide below is 500 nm. In the mid-infrared frequency range, the conductivity of graphene can be modeled with a semi-classical Drude model including the temperature correction (*T*=300K) [19] and should not be affected by the magnetic field oriented parallel to the graphene sheet [14] (along *z* axis in our case). The formula of conductivity can be expressed as [20],

$$\sigma(\omega) = \frac{2e^2}{\pi\hbar} k_B T \times \ln\left[2\cosh\left(\frac{\mu_c}{2k_B T}\right)\right]\frac{j}{\omega + j\tau^{-1}}, \quad (1)$$

where k_B is the Boltzmann constant, T is the temperature, μ_c is the chemical potential and ω is the angular frequency. The carrier relaxation time τ determines the carrier mobility *u* through $\tau = u\mu_c/ev_f^2$, where the *u*=10^4 cm^2/(V·s) is from the measured data [21] and has been involved in the previous investigations upon graphene plasmons [22]. The Fermi velocity is v_f =10^6 m/s [20], which was experimentally adopted in infrared nano-imaging [4]. When considering a system of multiple graphene layers with a spacing of 0.34 nm between each of them, such system can be regarded as a model of graphite as the spacing is significantly greater than the interatomic distance in graphene layer [19, 23]. And therefore the permittivity of graphite ε_g=2.5 is the lattice contribution to both the tangential permittivity $\varepsilon_{g,t}$ and surface-normal permittivity $\varepsilon_{g,n}$ of graphene. Meanwhile, by treating graphene as an ultrathin layer with thickness *d*=0.34 nm, the dynamical conductivity of graphene is included in the tangential permittivity term as $\varepsilon_{g,t}$=2.5-i$\sigma/\omega\varepsilon_0 d$ [20]. The surface-normal permittivity term is $\varepsilon_{g,n}$=2.5. The chemical potential of graphene is set as μ_c=0.45 eV, which can be implemented through chemical doping [24].

The magneto-optical effect has enabled a variety of non-reciprocal devices, whose optical properties are distinct for opposite directions of light propagation [25]. For the magneto-optical material InSb, the dielectric permittivity tensor under an external magnetic field *B* can be expressed as [14, 26],

$$\ddot{\varepsilon}_s \approx \varepsilon_\infty \begin{bmatrix} \varepsilon_{xx} & i\varepsilon_{xy} & 0 \\ -i\varepsilon_{xy} & \varepsilon_{yy} & 0 \\ 0 & 0 & \varepsilon_{zz} \end{bmatrix}, \quad (2)$$

where ε_∞=15.68 is the high-frequency permittivity. The tensor elements are $\varepsilon_{xx}=\varepsilon_{yy}=1-\omega_p^2/(\omega^2-\omega_c^2)$, $\varepsilon_{xy}=\omega_c\omega_p^2/\omega(\omega^2-\omega_c^2)$, $\varepsilon_{zz}=1-\omega_p^2/\omega^2$. The $\omega_p=[Ne^2/(\varepsilon_\infty\varepsilon_0 m^*)]^{1/2}$ and $\omega_c=eB/m^*$ are the plasma and cyclotron frequencies respectively. The electron density of doped InSb is *N*=2×10^{24} m^{-3}, which has been previously demonstrated in mid-infrared metamaterials [27] and could be implemented using Si or Be as the dopant and molecular beam expitaxy (MBE) technology [28]. The effective mass *m** is determined by *m**=0.012m_e at a temperature *T*=300 K [29], in which the constant m_e is the electron rest mass. Through the whole discussions in this paper, the maximum applied magnetic field is set as *B*=3T, which has been adopted in the previous experiments to describe magneto plasmons in monolayer graphene [30] and

magneto-optics effects in InSb materials [31-33]. The graphene plasmons propagation constant β_1 on InSb can be obtained by solving dispersion relation as [14],

$$\frac{\varepsilon_1}{k_2} + \frac{\varepsilon_{xx}^2 - \varepsilon_{xy}^2}{k_1\varepsilon_{xx} + \beta_1\varepsilon_{xy}} + \frac{i\sigma}{\omega\varepsilon_0} = 0, \qquad (3)$$

where $k_1 = \sqrt{\beta_1^2 - \left[\omega^2(\varepsilon_{xx}^2 - \varepsilon_{xy}^2)/\varepsilon_{xx}\right]/c^2}$ and $k_2 = \sqrt{\beta_1^2 - (\varepsilon_1\omega^2/c^2)}$. With an external magnetic field B, the ε_{xy} in the denominator of 2nd term would be non-zero. Therefore opposite plasmon propagation directions (*i.e.* propagation constant β_1 with opposite signs) leads to different plasmons modal indices, which provides the non-reciprocal functionality of proposed structure. Derived from Eqs. (1-3), the real modal indices of GPs along opposite traveling directions on GNW as functions of the wavelength and external magnetic field are presented in Fig. 2. The modal indices are defined as the ratio between graphene plasmons and vacuum propagation constants. External magnetic fields for two cases are B=3T in Fig. 2(a) and incident wavelength is 8.5μm in Fig. 2(b).
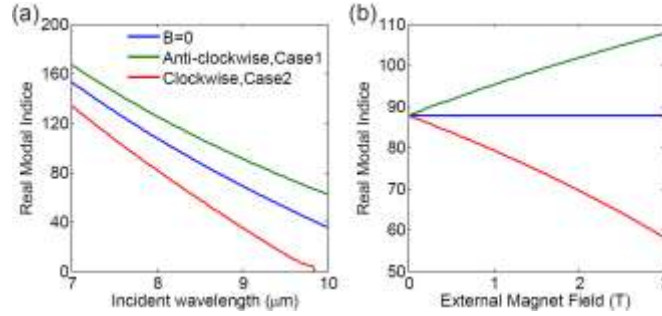

Fig. 2. Dependencies of the real modal indices of plasmons on a GNW with anti-clockwise and clockwise traveling directions on wavelengths (a) with B=3T and on external magnetic field B (b) with wavelength 8.5μm. For comparison, the real modal indices without external magnetic bias are shown as well.

As shown in Fig. 2(a), the real modal indices of all three cases decrease as the wavelength increases. Compared with the modal indices of GPs under B=0, the counterparts with anti-clockwise (clockwise) traveling direction possess higher (lower) values. As the wavelength further increases to 10 μm, the GPs with clockwise traveling direction are no longer supported on the GNW. Meanwhile, it is worth noting that the plasmons wavelengths λ_{spp}, which can be derived from the ratio between incident wavelength and real modal indices of GPs, also present similar trends to those in Fig. 2(a). Figure 2(b) presents the evolution of real modal indices with respect to the increase of external magnetic field B. As the external magnetic field increases from zero to B=3T, real modal indices increase or decrease for Case 1 or Case 2, splitting from the reference value with no magnetic bias. Such non-reciprocal dispersion relation of GPs on InSb GNW provides us chances to achieve a magnetically tunable plasmon filter with a non-reciprocal transmittance spectrum.

3. Magnetically tunable non-reciprocal plasmons filter

It is well known that for a filter composed of a resonator ring coupled with a waveguide, the resonant wavelength λ_{res} can be simply expressed via resonant cavity theory,

$$2\pi R = M\frac{\lambda_{res}}{N_{eff}}, (M = 1,2,3,...), \qquad (4)$$

in which the R is radius of InSb nanowire, M is the resonant mode order, λ_{res} is the resonant wavelength and N_{eff} are the modal indices of the graphene plasmons. As shown in Fig. 2,

when an external magnetic field is applied, the real modal indices of the GPs change and the dispersion relations of GPs on GNW become non-reciprocal. Therefore, under an external magnetic field, a non-reciprocal shift of filter transmittance spectrum can be expected as input plasmons are along opposite directions. To present this non-reciprocal spectrum shift, we show the transmittance (in units of dB) under opposite input directions with magnetic field $B=$ 3T in Fig. 3. For comparison, the results without external magnetic field are shown in dashed lines. In Figs. 3(a) and 3(b), the plasmons input from Port #1 (Case 1) and Port #2 (Case 2), respectively. Here we denote the period number of magnetic field component H_z as the order of resonant mode. In the figures only five orders of resonant modes (order 4th to 8th with corresponding transmittance dips distribute from longer to shorter wavelength) are presented with the H_z field profile of 4th mode of Case 2 is shown in the inset.
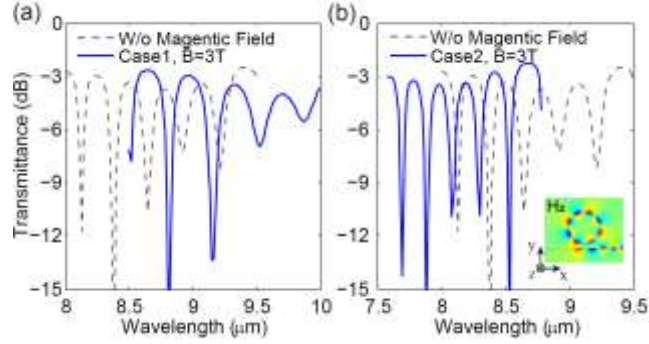

Fig. 3. The transmittance spectra (in units of dB) obtained from numerical simulations for plasmons input from Port #1 (a) [Case 1 of Fig. 1(a)] and Port #2 (b) [Case 2 of Fig. 1(b)]. Meanwhile, the results for the case without magnetic field are plotted with dashed lines. The external magnetic field is $B=$3T. The H_z field profile of 4th mode in Case 2 is shown in the inset.

As shown in the figures, under an external magnetic field, the transmittance spectra of Case 1 shifts to longer wavelength while the one of Case 2 shifts to shorter wavelength, which can be explained through Eq. (4) and Fig. 2. As shown in Fig. 2(b), the real modal indice N_{eff} increases or decreases with the external magnetic field for Case 1 or Case 2. For the same order of resonant mode (parameter M is fixed) in Eq. (4), the increase of N_{eff} leads to larger λ_{res}, meaning the spectrum shifts to longer wavelength region. Similarly, the decrease of N_{eff} for Case 2 leads to the smaller λ_{res}, meaning the spectrum shifts to shorter wavelength region. Meanwhile, the amplitude of spectrum for each order of resonant mode changes. This phenomenon can be attributed to two reasons. At short wavelength and no external magnetic field, the graphene plasmons present stronger field confinement and therefore weaker coupling between the graphene sheet waveguide and GNW structure and larger transmittance (e.g. near λ=8.15 μm). At long wavelength, the plasmons attenuation is lower due to weaker field confinement and the transmittance would be also larger (e.g. near λ=9 μm). Once an external magnetic field is applied, the higher external magnetic field leads to stronger modal confinement and larger attenuation for Case 1[see Fig. 2(b)], similar to the situation under smaller wavelength. In contrast, for Case 2, higher magnetic field leads to weaker modal confinement and smaller attenuation, similar to the situation under longer wavelength. Therefore, the variations of amplitude in spectrum originates from the combinations of effects of coupling strength and plasmons attenuation.

As for the performances of such device, the insertion loss is around 3 dB and could be attributed to the small graphene chemical potential and long traveling distance of plasmons due to the large nanowire radius. Higher chemical potential as well as more compact device dimensions would be beneficial for better performance, although these may increase the fabrication complexity. As for the bandwidth of filter, a narrow bandwidth with a half-maximum bandwidth around 100 nm can be achieved in the proposed filter. On the other hand,

due to the intrinsic properties of GPs on magneto-optical substrates [14], reversing the input direction of plasmons has the same effect as reversing the external magnetic field direction, figure 3(b) could also be regarded as the situation of Case 1 with B=-3T. Therefore the external magnetic field endows such filter a tunability with magnetic field from B=-3T to B=3T. For instance, the resonant wavelength of 7th mode in Case 1 can be tuned from λ_{res}=7.8 μm under B=-3T to λ_{res}=8.8 μm under B=3T with an adjustable range around 1 μm.

To describe the resonances of plasmons on the GNW resonator, we have obtained the resonant wavelengths via solving Eqs. (3) and (4) with the results are shown in Fig. 4(a), in which the dashed lines are the real modal indices for five orders of resonances from Eq. (4) and the solid lines are from Eq. (3). The crossover points in Fig. 4(a) are presented via star markers in Fig. 4(b). For comparisons, the resonant wavelengths from numerical results of Figs. 3(a) and 3(b) are illustrated via square markers.
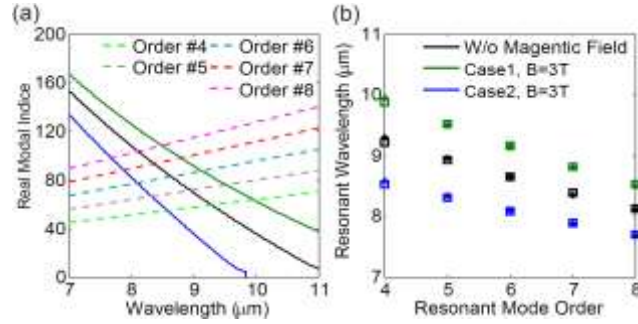

Fig. 4. The real modal indices on from Eq. (3) (solid lines) and Eq. (4) (dashed lines) are shown in (a). The crossover points in (a) and the resonant wavelengths from numerical simulations are illustrated using star markers and square markers, respectively.

As shown in Fig. 4(a), the resonant wavelength of a specific resonant order without magnetic field is located between the values under magnetic field B=3T with opposite input directions. Specifically, for each order of resonant mode, the resonant wavelength of Case 2 (Case 1) is the shortest (longest). On the other hand, for each case, the resonant wavelength decreases as the resonant order number increases. In Fig. 4(b), we could observe that the resonant cavity theory shows good agreement with the numerical solutions.

4. Magnetically tunable plasmons isolator

As shown in the previous discussion, the transmittance spectrum could be tuned by external magnetic field where the shift direction is determined by plasmons input direction. Thus at one wavelength, it is possible that plasmons could pass along one of the two input directions while being filtered along the other. In such a situation, the plasmons filter performs as an isolator. To describe the performance of isolator, we first denote the isolation ratio we use in the discussion below. The isolation ratio can be obtained by making a difference between the transmittances of two cases in Fig. 3. In this paper, the isolation ratio is defined as *IR=Transmittance* (Case 2)-*Transmittance* (Case 1). Since the transmittance spectrum of filter is magnetically tunable, the *IR* ratio could also be dynamically controlled. To illustrated this tunability, we present the *IR* ratios as a function of incident wavelengths under two lower magnetic fields B=1T and B=2T in Fig. 5(a). The wavelength spans from 7.5 μm to 9.5 μm. Furthermore, we have investigated the dependences of isolation ratios on various external magnetic fields, ring radii and graphene chemical potentials under two different incident wavelengths in Figs. 5(b-d). The incident wavelengths are chosen as λ=8.2 μm and λ=8.5 μm, which correspond to the highest and lowest isolation ratio cases under B=1T in Fig. 5(a), respectively. The external magnetic field spans from B=0.1 T to B=3 T in Fig. 5(b), ring radius spans from 50 nm to 150 nm in Fig. 5(c) and the chemical potential spans from μ_c=0.3

eV to μ_c=0.45 eV. Without detailed explanations, the parameters are set as B= 1 T, R= 100 nm and μ_c=0.45 eV.

Figure 5(a) shows that the isolation ratio can be adjusted by an external magnetic field. With the increase of magnetic field, the spectrum of isolation ratio presents a redshift. Specifically, the isolation ratio could be more than 25 dB with the wavelength near 8.5 μm and the magnetic field B=1T. As shown in Fig. 5(b), for each incident wavelength, several peaks or dips can be observed. It is worth noting that changing the external magnetic field would lead to the switch of enabled propagation direction (represented by the sign of isolation ratio), although the corresponding amplitudes are different. For instance, at λ=8.5 μm, the isolation ratio can be near 25 dB under B=1 T with the enabled propagation direction along x^+ axis. However, to achieve the enabled propagation direction along x^- axis by adjusting the amplitude of magnetic field, only the isolation ratio near 10 dB is obtained under B=3T. In contrast, the enabled propagation direction along x^- axis with isolation ratio as 25 dB can be obtained by simply reversing the magnetic field direction (*i.e.* B=-1T) due to the intrinsic principle of non-reciprocal dispersion [14], which provides another route to achieve the switch of enabled propagation direction. Therefore in the practical applications, reversing the external magnetic field direction would be more efficient than simply adjusting the amplitude of magnetic field.
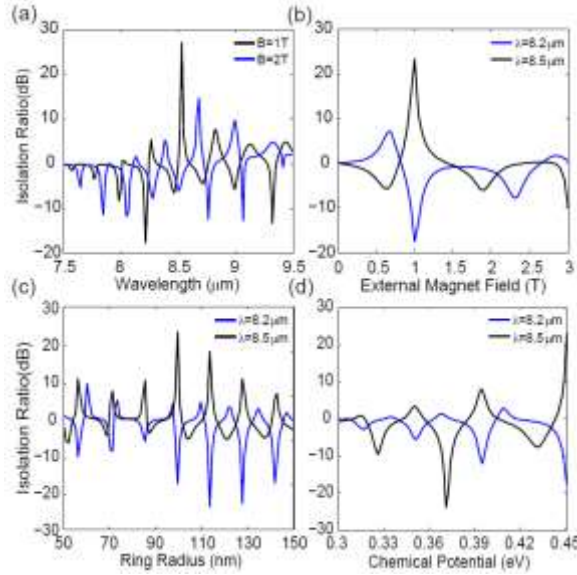

Fig. 5. The isolation ratio as functions of incident wavelength under different applied magnetic fields (a) and of applied magnetic field (b), ring radius (c) and chemical potential (d) under different incident wavelengths (λ=8.2 μm and 8.5 μm).

As shown in Fig. 5(c), with the increasing of ring radius, the periodical modulations of isolation ratios can be observed for both wavelengths. Each of these isolation ratio peaks or dips corresponds to one resonant mode and all these peaks or dips are distributed equidistantly. This can be explained by Eq. (4), in which the resonant mode order M is linearly dependent on the radius R provided that other parameters are fixed. The highest isolation ratio for λ=8.5 μm is located at R=100 nm while the lowest isolation ratio for λ=8.2 μm is located at near R=115 nm. In Fig. 5(d), higher isolation ratio can be achieved under larger chemical potential. The reason behind this is the lower chemical potential brings higher field confinement and therefore weaker coupling between ring cavity and sheet waveguide, which means there is more energy of plasmons coupled to the output port at the resonant wavelength. It is also

worth noting that, higher chemical potential causes less modal attenuation and insertion loss. The investigation on ring radius and chemical potential can be carried out before the fabrication of isolator according to achieve better performance. For better presentation, we have added the comparison between magnetic isolators in this paper and the ones proposed in literatures. The results are shown in the Table below.

Table 1. Performance comparisons of magnetically tunable plasmons isolator to literature values of graphene magnetic isolators

Operation Frequency	Magnetic Bias	Extinction Ratio	Insertion Loss	Ref.
Microwave	0~5 T	~25 dB	~5 dB	[34]
Mid-infrared	~4 T	~25 dB	~4 dB	[35]
Terahertz	0~1 T	~23 dB	~3 dB	[36]
Mid-infrared	0~2 T	~25 dB	~3 dB	Fig.5

As shown in the table, for the mid-infrared frequency regime, the plasmons isolator proposed in this paper could achieve comparable extinction ratio to the previously reported devices while with less insertion loss and lower magnetic field bias. As is mentioned, the enabled pass direction for such isolator could also be adjusted by reversing the magnetic field direction. To reveal this, we have shown the field profiles of the 6th resonant modes at the peak near 8.5 μm for two cases under B=1T and B=-1T in Fig. 6. The red arrows illustrate the plasmons power flow direction. As shown in the two profiles of Figs. 6(a-b). The graphene plasmons which incident at Port #1 could not pass such a filter due to the resonances in the GNW resonator. In contrast, the plasmons incident at Port #2 can be coupled to the GNW and then continue to output from Port #1 due to the fact that resonant condition is not established. Once the external magnetic field direction is reversed, the enabled pass direction is switched to that from Port #1 to Port #2, as shown in Figs. 6(c-d).
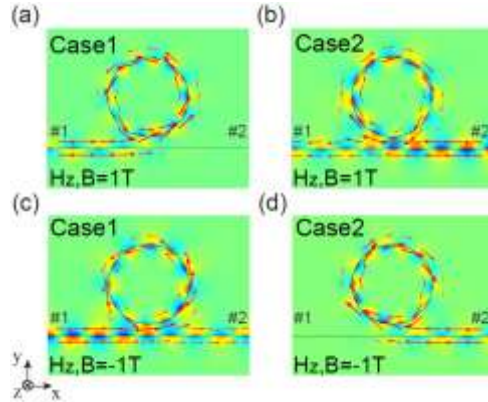

Fig. 6. The profiles of magnetic field component H_z of Case 1 and Case 2 under magnetic field B=1T (a,b) and B=-1T (c,d) at λ=8.5μm. The order of resonant mode is 6th. The red arrows illustrate the plasmons power flow direction.

Conclusion

In this paper, we propose a magnetically tunable non-reciprocal plasmons resonator based on a graphene-coated InSb nanowire. When coupled with a graphene sheet waveguide and with an applied external magnetic field, graphene plasmons on the magneto-optical nanowire have different modal indices with respect to the traveling directions. Correspondingly, the shift of transmittance spectrum of such a filter becomes non-reciprocal and magnetically tunable. The shift of resonant wavelengths in spectrum can be well explained by resonant cavity theory. Furthermore, the non-reciprocal transmittance also enables the filter to achieve the function of

an isolator. Moreover, the isolation ratio of such isolator could be tuned by an external magnetic field with the enabled pass direction being reversed by reversing the magnetic field direction. Specifically, an isolation ratio above 25 dB can be obtained. The proposed magnetically tunable non-reciprocal resonator may provide new possibility to dynamically control plasmons in devices based on graphene-coated nanowires.

Acknowledgment